Optics Communications 483 (2021) 126601

Contents lists available at ScienceDirect

Optics Communications

journal homepage: www.elsevier.com/locate/optcom

# Phase error analysis of clipped waveforms in surface topography measurement using projected fringes

Kjell J. Gåsvik [a,*], Kjell G. Robbersmyr [a], Trond Vadseth [b]

[a] Faculty of Engineering and Science, Department of Engineering Science/Mechatronics, University of Agder, N-4886 Grimstad, Norway
[b] SINTEF Digital, Norway

ARTICLE INFO

*Keywords:*
Optical metrology
Projected fringes
Phase shift
Signal processing
Profilometry
3-D measurement
Fourier analysis
Phasor diagrams

ABSTRACT

When working with the method of projected fringes outside the optical laboratory one often encounters the problem of uncontrollable ambient light. This might cause saturation of the camera which in turn results in clipping of the fringes. Since standard theories describing phase-shifting techniques assume the projected fringes to be purely sinusoidal, such clipping will result in measurement error. In this paper a detailed analysis of this problem is given, and relations between phase errors, the amount of fringe clipping and the number of phase steps are found. Moreover, the phase difference between the clipped and the unclipped fringes is described. This investigation is based on Fourier- and phasor analysis.

## 1. Introduction

In optical measurement techniques like classical and holographic interferometry, moiré and speckle methods, one faces the problem of analyzing a set of fringes, called interferograms. In the present paper we shall concentrate on the method of projected fringes.

A short glance at the specifics of the projected fringe method is shown in Fig. 1 where a typical experimental set up is sketched. A light ray from the projector hits the object- and reference surface (the xy-plane) at two different points. The distance between these two points along the $x$-axis is u, as seen by the camera. From the figure we find that the height difference $z = u/(\tan\upsilon_0 + \tan\upsilon)$. We further have that $\theta = u/p$, where $\theta$ is the phase and $p$ is the period of the projected sinusoidal fringes. With plane wave illumination and the camera focused at infinity, it can be shown that $z = p\theta/\tan\upsilon_0$. By this method one can measure the topography of surfaces, deformations, etc. A more comprehensive description of the projected fringe method can be found in [1] and a lot of references to applications of the method can be found in [2].

In the projected fringe method, (also termed the structured light method) a periodic fringe pattern is projected onto the surface under investigation. This fringe system represents a carrier wave. When the surface is curved, or in other ways deviate from a reference surface, this carrier will be modulated by a phase function which contains, as we have seen, information about the topography of the surface. To unveil this information, the carrier has to be demodulated.

Rather than determining the phase function directly, it has in recent years been common to analyze it indirectly by measuring the intensity of the fringes. This method of demodulation is called the phase-shifting or phase-stepping technique. In Section 2, we go through the theory of this method.

The standard theories describing the phase-shifting technique, assume the projected fringes to be purely sinusoidal. This is not always strictly correct in practice. One of the reasons for this are non-linearities in the projector and/or camera [3,4]. Some authors have studied the case of non-sinusoidal fringes in general [5,6] ,specifically when defocusing the image of a rectangular grating onto the surface [7].

Apparatus based on the projected fringe method has in many cases moved out from the optical laboratory into industrial environments. Then one often encounters the problem of uncontrollable ambient light. Also, measuring shiny metal surfaces might be a problem. This can result in saturation of the camera which in turn results in clipping of the fringes. Image saturation has been studied and analyzed by many authors [8–11]. This effect is also studied experimentally [12] where the measurement error was recorded as a function of a controlled background illumination.

In this paper we will investigate the relation between the phase error and the amount of clipping with different number of phase steps. In addition, the phase difference between the clipped and the unclipped fringes will be described. The study is based on Fourier- and phasor analysis.

* Corresponding author.
*E-mail address:* kgasvik@goose.no (K.J. Gåsvik).

https://doi.org/10.1016/j.optcom.2020.126601
Received 26 August 2020; Received in revised form 2 November 2020; Accepted 8 November 2020
Available online 11 November 2020

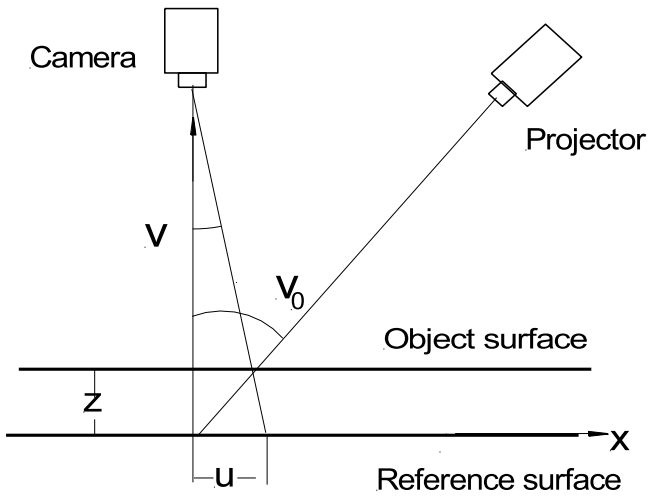


**Fig. 1.** Experimental set up for the projected fringe method. The camera is coupled to a PC.

## 2. The phase-shift method. Fringe clipping

Let the intensity distribution of the ideal, sinusoidal fringes be given by

$$I = a + b\cos\theta \tag{1}$$

The problem is to recover the phase $\theta$ which is related to the surface topography.

In phase shift methods [13–17], an experimentally controllable phase $\alpha_i$ is introduced such that

$$I_i = a + b\cos(\theta + \alpha_i) \tag{2}$$

Here $i = 1, 2, \ldots N$, where $N$ is the number of phase steps.

$$\text{Let } \alpha_i = \frac{i2\pi}{N} \tag{3}$$

Which means that each period is divided into $N$ equal steps. By using the least squares method, it can be shown that

$$\tan\theta = \frac{-\sum_{i=1}^{N} I_i \sin(i2\pi/N)}{\sum_{i=1}^{N} I_i \cos(i2\pi/N)} \tag{4}$$

Clipping of sinusoidal signals is a well-known phenomenon in signal processing. There it is termed harmonic distortion. The case we shall study is unsymmetrical clipping and is shown in Fig. 2.

Fig. 2 shows one period of a clipped cosine-function which we denote $g(x)$. The magnitude of the clipping is given by the clipping angle $\phi$. One way of describing this fringe function is to write it as a Fourier series. Since $g(x)$ is symmetric, we get

$$g(x) = c_0 + \sum_{k=1}^{\infty} c_k \cos(kx) \tag{5a}$$

where

$$c_k = \frac{1}{\pi}\int_{-\pi}^{\pi} g(x)\cos(kx)dx = \frac{2}{\pi}\int_{0}^{\pi} g(x)\cos(kx)dx \tag{5b}$$

By solving the following integrals:

$$c_k = \frac{2}{\pi}\left[\cos\varphi\int_0^{\varphi}\cos(kx)dx + \int_{\varphi}^{\pi}\cos(x)\cos(kx)dx\right] \tag{6}$$

we get

$$c_k = \frac{1}{\pi}\left[2\cos\phi\frac{\sin k\phi}{k} - \frac{\sin(k+1)\phi}{k+1} - \frac{\sin(k-1)\phi}{k-1}\right] \text{ for } k>1 \tag{7a}$$

$$c_0 = \frac{2}{\pi}\left[\phi\cos\phi - \sin\phi\right] \tag{7b}$$

$$c_1 = \frac{1}{\pi}\left[\pi - \varphi + \frac{1}{2}\sin 2\varphi\right] \tag{7c}$$

Fig. 3 shows $c_k$ as a function of $k$ for $k > 1$. $c_k$ is of course not a continuous function, but written as such, the trend of the coefficients is better visible. We see that the Fourier coefficients $c_k$ for $k > 4$ are so small that a good approximation of $g(x)$ would be

$$g_4(x) = c_0 + \sum_{k=1}^{4} c_k\cos(kx) \text{ which we denote } g_4. \tag{8}$$

Fig. 4 shows the Fourier coefficients $c_0$–$c_4$ as a function of the clipping angle $\phi$. As seen, we take $\phi \in [0, \pi/2]$. It would be very unusual in practice to work with a clipping angle greater than that.

Fig. 5 shows a graph of $g_4$ with a clipping angle $\phi = \pi/3 = 60°$. Also shown is $\cos(x)$.

At first sight, it might look as the whole positive part of $\cos x$ will be clipped when $\phi = \pi/2$, i.e., $g_{4\max} = 0$. In fact, this configuration occurs at a lower value of $\phi$. We know that $g_4$ has a maximum at $\theta = 0$. Inserting this value into Eq. (8), we get

$$\sum_{k=0}^{4} c_k = 0$$

which gives $\phi = 1.35$ rad. This situation is shown in Fig. 6.

Note that here we have changed the name of the variable from $x$ to $\theta$, the same $\theta$ as in Eq. (1). This representation will be used in the rest of this manuscript.

## 3. Errors in phase measurements

Now we should be able to calculate the new phase by using the function g instead of $I$ in Eq. (4). A first step would be to simplify this equation, at least for the lower values of $N$. We find for $N = 4$:

$$\tan\theta = \frac{I_1 - I_3}{I_4 - I_2} \tag{9}$$

The expressions for $N = 3, 5$ and 6 are a bit more complicated. To find the new phase $\psi$, we then have to insert $I_i = g_{4i}$ into these expressions. This is a rather cumbersome and risky (for errors) process. Fortunately, an excellent paper written by Su et al. [7] came to our assistance. They have developed a general formula valid for unspecified Fourier coefficients and unrestricted number of phase steps. In our terminology and with $k_{\max} = 4$, it reads:

$$\tan\psi = \frac{c_1\sin\theta_1 - c_{N-1}\sin(N-1)\theta + c_{N+1}\sin(N+1)\theta}{c_1\cos\theta_1 + c_{N-1}\cos(N-1)\theta + c_{N+1}\cos(N+1)\theta} \tag{10}$$

where $\psi$ is the new phase for the clipped cosine function.
With this formula in hand, we get for $N$ up to 6:

$$\tan\psi(N=3) = \frac{c_1\sin\theta - c_2\sin(2\theta) + c_4\sin(4\theta)}{c_1\cos\theta + c_2\cos(2\theta) + c_4\cos(4\theta)} \tag{11a}$$

$$\tan\psi(N=4) = \frac{c_1\sin\theta - c_3\sin(3\theta)}{c_1\cos\theta + c_3\cos(3\theta)} \tag{11b}$$

$$\tan\psi(N=5) = \frac{c_1\sin\theta - c_4\sin(4\theta)}{c_1\cos\theta + c_4\cos(4\theta)} \tag{11c}$$

$$\tan\psi(N=6) = \frac{c_1\sin\theta}{c_1\cos\theta} = \tan\theta \tag{11d}$$

Now we are able to find the measurement error $\Delta\theta$ through

$$\Delta\theta = \psi - \theta = \arctan(\tan\psi) - \arctan(\tan\theta) \tag{12}$$

A result of this procedure is shown in Fig. 7. Here $N = 3$, $\phi = 45°$. We see that the error varies between $\pm 0.05$. The same is done for $N = 3, 4$ and 5, for different values of the clipping angle $\phi$ and the results are given in Table 1. There we also have listed the dependence of the phase error on the clipping height $h$ and number of phase steps $N$. The clipping height is given as $h = 1 - \cos\phi$, i.e. the fraction of the amplitude. We have only considered clipping heights of practical interest.

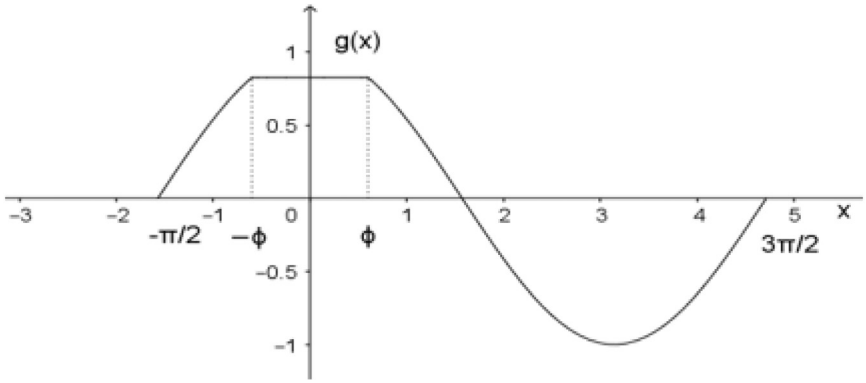


**Fig. 2.** Clipped cosine. $\phi$ = the clipping angle.

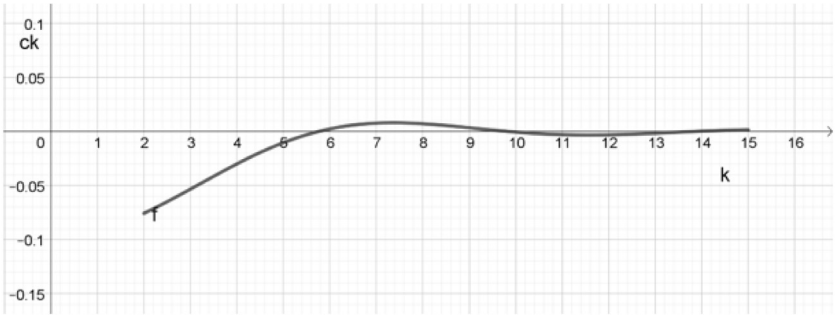


**Fig. 3.** $c_k$ as a function of $k$. for $k > 1$ and $\phi = \pi/4$.

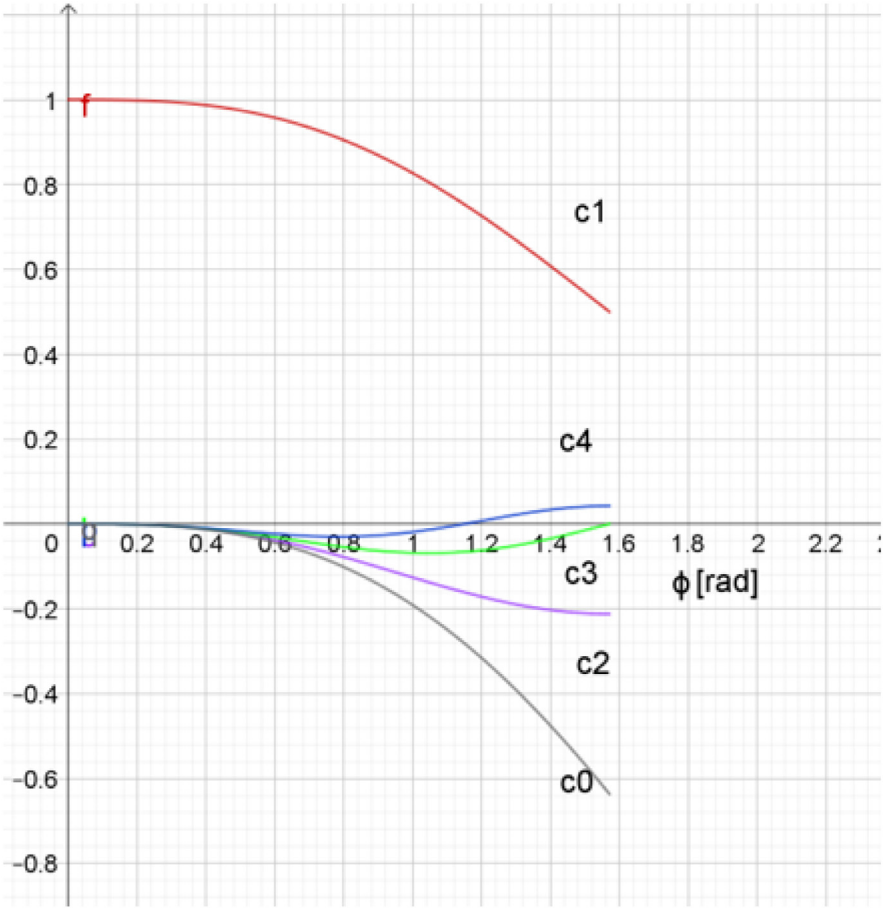


**Fig. 4.** The Fourier coefficients $c_0$–$c_4$ as a function of the clipping angle $\phi$.

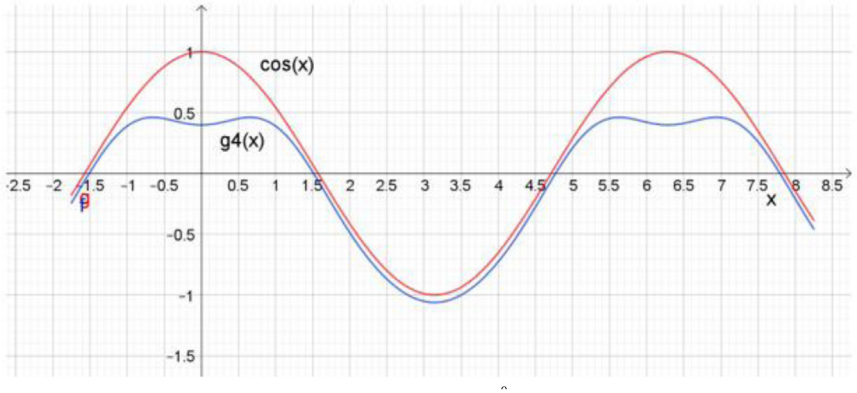


**Fig. 5.** Graph of $g_4(x)$ and $\cos(x)$. $\phi = \pi/3 = 60°$. Amount of clipping = 50%.

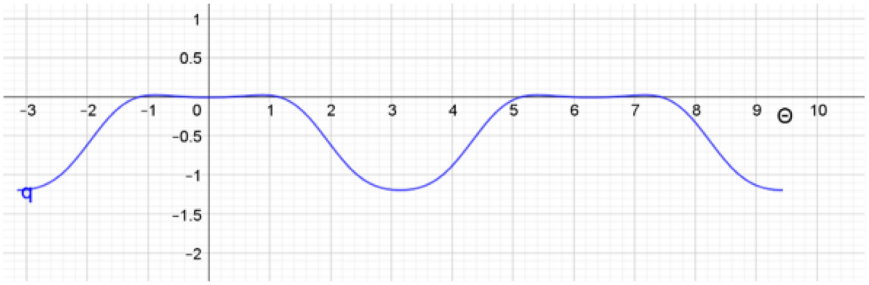


**Fig. 6.** $g_4(\theta)$ for $\phi = 1.35$ rad $= 77.3°$ showing that the whole function is negative.

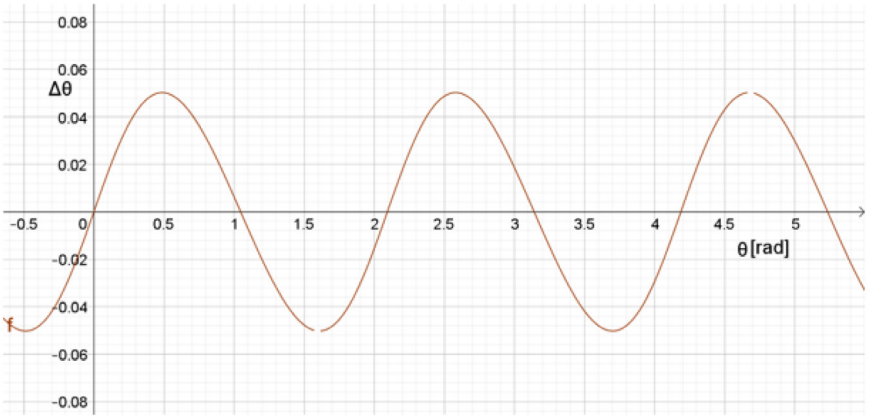


**Fig. 7.** $\Delta\theta$ as a function of $\theta$. $N = 3$, $\phi = \pi/4 = 45°$.

**Table 1**
Phase error (in rad) as function of phase steps $N$, the clipping angle $\varphi$, and the clipping height $h$.

| * | $\varphi$[deg] | 30 | 36 | 45 | 60 |
|---|---|---|---|---|---|
| | $h$ (%) | 13 | 20 | 30 | 50 |
| $N = 3$ | $\Delta\theta_{max}$ | 0.01 | 0.02 | 0.05 | 0.28 |
| | RMS | 0.007 | 0.014 | 0.035 | 0.20 |
| $N = 4$ | $\Delta\theta_{max}$ | 0.02 | 0.04 | 0.06 | 0.09 |
| | RMS | 0.014 | 0.028 | 0.04 | 0.06 |
| $N = 5$ | $\Delta\theta_{max}$ | 0.02 | 0.03 | 0.03 | 0.02 |
| | RMS | 0.014 | 0.02 | 0.02 | 0.014 |

**Table 2**
Phase difference $\Delta\omega$ (in rad) between the clipped and unclipped fringe function.

| $\varphi$[deg] | 30 | 36 | 45 | 60 |
|---|---|---|---|---|
| $h$ (%) | 13 | 20 | 30 | 50 |
| $\Delta\omega_{max}$ | 0.04 | 0.075 | 0.08 | 0.14 |
| $\Delta\omega_{RMS}$ | 0 | 0.014 | 0.034 | 0.097 |
| $\Delta\omega_{max}/\sqrt{2}$ | 0.028 | 0.053 | 0.057 | 0.097 |

## 4. Phasor diagrams

In the preceding sections we have found the measuring error subject to certain approximation ($k_{max} = 4$). It would be interesting to find the phase deviation induced by the same approximation. To do that, we have to transform $g_4$ into the form $R\cos\beta$. This can be done by constructing a phasor diagram. A phasor is represented as a vector in the complex plane. The method of phasor addition we will use can be employed without any appreciation of its relationship to the complex number formalism.

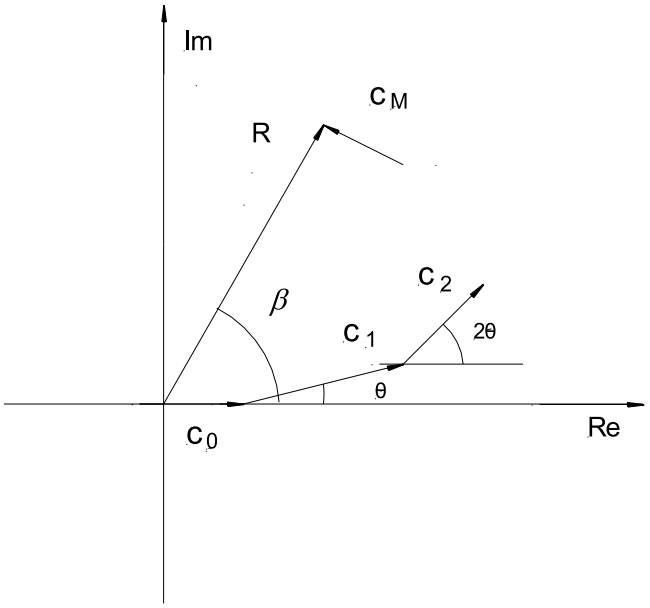


**Fig. 8.** Phasor diagram (symbolically) of the first $M$ terms of a Fourier series. The lengths of the phasors are arbitrary, but the phasor angle increases by $\theta$ for each step.

Let us denote the sum of the first $M$ terms of a Fourier series of an even function $g_M(\theta)$. Then we have (see Fig. 8)

$$g_M(\theta) = R\cos\beta, \text{where} \tag{13}$$

$$\tan\beta = \frac{\sum_{k=1}^{M} c_k \sin(k\theta)}{c_0 + \sum_{k=1}^{M} c_k \cos(k\theta)} = \frac{Y}{X} \text{ and} \tag{14}$$

$$R = \left[\left(c_0 + \sum_{k=1}^{M} c_k \cos(k\theta)\right)^2 + \left(\sum_{k=1}^{M} c_k \sin(k\theta)\right)^2\right]^{\frac{1}{2}} = \sqrt{X^2 + Y^2} \tag{15}$$

Where we have introduced the shorthand notation

$$X = c_0 + \sum_{k=1}^{M} c_k \cos(k\theta) \text{ and } Y = \sum_{k=1}^{M} c_k \sin(k\theta)$$

To test the validity of our calculation, we have

$$\cos\beta = \frac{1}{\sqrt{1+\tan 2\beta}} = \frac{X}{\sqrt{X^2+Y^2}} \text{ which gives}$$
$$R\cos\beta = \sqrt{X^2+Y^2}\frac{X}{\sqrt{X^2+Y^2}} = X$$

This is not a strict proof, but confirms Eqs. (14), (15).

We now turn back to our clipped cosine function and $M = 4$. In the same way as above, we now can calculate the deviation $\Delta\omega = \beta - \theta$

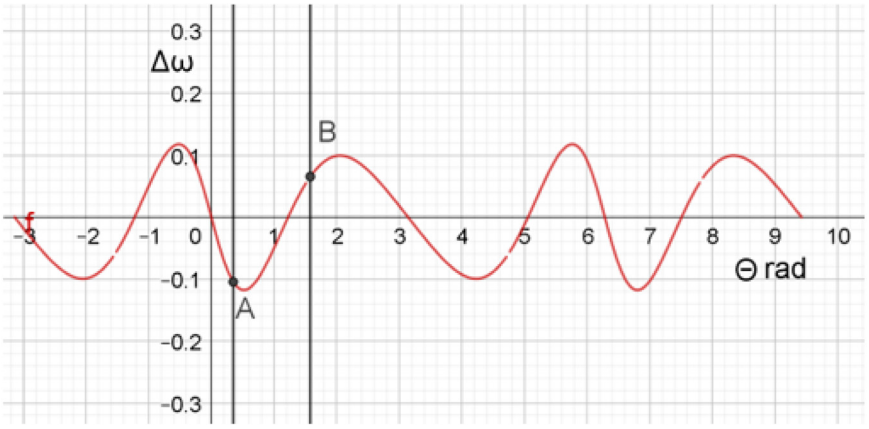


**Fig. 9.** Phase difference $\Delta\omega$ (in rad) between clipped and unclipped fringe functions. $M = 4$, $\phi = \pi/3 = 60°$.

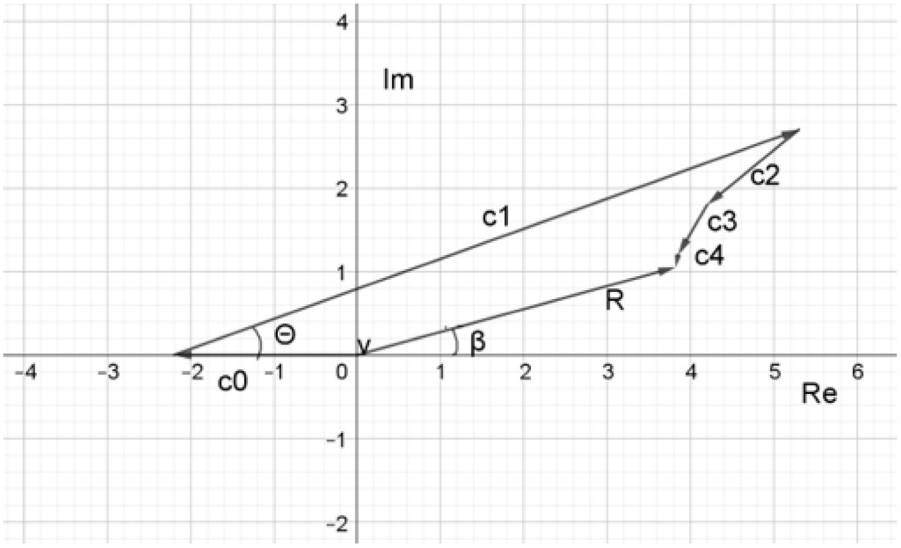


**Fig. 10.** A real phasor diagram of $g_4$.$\theta = 20° = 0.35$ rad, $\phi = \pi/3 = 60°$ $R$ is the resultant phasor. $c_4$ is barely visible.

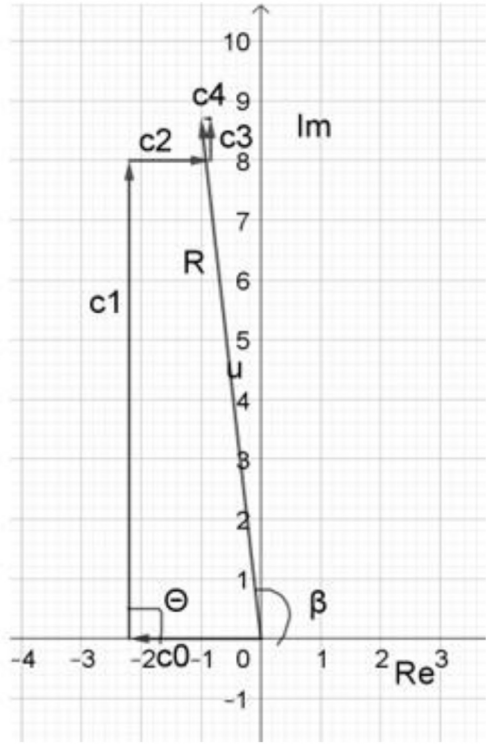


**Fig. 11.** Phasor diagram. $\theta = \pi/2 = 90°$, $\phi = \pi/3$. $c_4$ is barely visible.

induced by our approximation by calculating

$$\Delta\omega = \beta - \theta = \arctan(\tan\beta) - \arctan(\tan\theta) \tag{16}$$

An example is shown in Fig. 9, with $M = 4$, $\phi = \pi/3$. Her we see that the deviation varies between $\pm 0.12$ rad.

Eq. (16) is calculated for different values of the clipping angle $\phi$, and the results are given in Table 2.

In Fig. 10 we have made a real phasor diagram of $g_4$. Here $\phi = \pi/3$ and $\theta$ is set to 20°. The resultant phasor is making an angle $\beta$ to the $x$-axis. If we had $\beta = \theta$, i.e. $R$ parallel to $c_1$, $g_4$ would have the same phase as $\cos\theta$. In the diagram, we can measure the angle between $c_1$ and $R$ $(= \theta - \beta)$ to be 5° = 0.09 rad. The same can be found from the graph in Fig. 9. The point A with $\theta = 20° = 0.35$ rad is marked, and we can read off a deviation of 0.10 rad. It is clear that this method gives a better accuracy that reading off the angle from a phasor diagram. The discrepancy is however, remarkably low.

Fig. 11 shows another phasor diagram of $g_4$. Here $\theta = \pi/2$, $\phi = \pi/3$. By measuring the angle between $c_1$ and R, we determine $\beta - \theta$ to be 6° = 0.1 rad. In the graph of Fig. 9, we find at the marked point B, $(\theta = 90° = \pi/2$ rad), the same quantity to be 0.07 rad.

Another test is to compare the length of $R$ given by Eq. (15) and displayed by the graph in Fig. 12, with the same length given in the phasor diagrams.

The two marked points in the graph are A ($\theta = 20° = 0.35$ rad) and B ($\theta = 90° = \pi/2$ rad). We find $R_A = 0.41$ and $R_B = 0.88$ which agree very well with same quantities found in the phasor diagrams in Figs. 10 and 11.

## 5. Discussions

As seen, the measurement error and the phase differences are represented by the maxima of the functions $\Delta\theta$ and $\Delta\omega$. The root mean square (RMS) is another way of representing the same quantities. For harmonic functions, the RMS is given as $a/\sqrt{2}$, where $a$ is the amplitude. The $\Delta\theta$-functions are harmonic, see e.g. Fig. 7. Therefore, we have used this expression to calculate the RMS and filled it into Table 1.

The $\Delta\omega$– functions, however, are not harmonic, see e.g. Fig. 9. To find the RMS, we therefore have to integrate the square of $\Delta\omega$ over one period. A problem is that these functions have singularities seen as small gaps in the graphs. The reason is that the function $\arctan(\tan(x))$ has singularities at $x = \pi/2$ and $3\pi/2$. The solution is to divide the integrand into 3 parts and jump past the singularities. The resulting error will be negligible. The results are given in Table 2.

To name $\Delta\theta$ the measuring error is a bit of a misnomer, but is widely accepted in the literature. When measuring the phase of the clipped fringes, one should expect the error to be equal to $\Delta\omega$. By comparing the RMS-values of $\Delta\theta$ and $\Delta\omega$ in Tables 1 and 2 for $N = 5$, we see that this is in fact correct, except for the extreme case of $h = 50\%$.

So, what does these measuring errors imply when performing surface topography measurements? For simplicity we apply parallel illumination and a projection angle equal to 45°. Then the height measuring error $\Delta z$ is given by

$$\Delta z = \frac{p}{\tan(45°)}\Delta\theta = p\Delta\theta$$

Where $p$ is the period of the projected fringes. In this case, $\Delta z$ is given as the fringe period times $\Delta\theta$ in radians.

## 6. Conclusions

To study the effect of fringe clipping in phase-shifting fringe projection profilometry, the clipped fringe function is expanded into a Fourier series. From this series, we have found the resulting phase error as a function of h, the clipping height and N, the number of phase steps. Our results show that

(1) For clipping height below ~20% of the amplitude, the phase error is of the same order of magnitude as other sources of error (surface reflectivity, electronic noise, gamma nonlinearity, etc.)

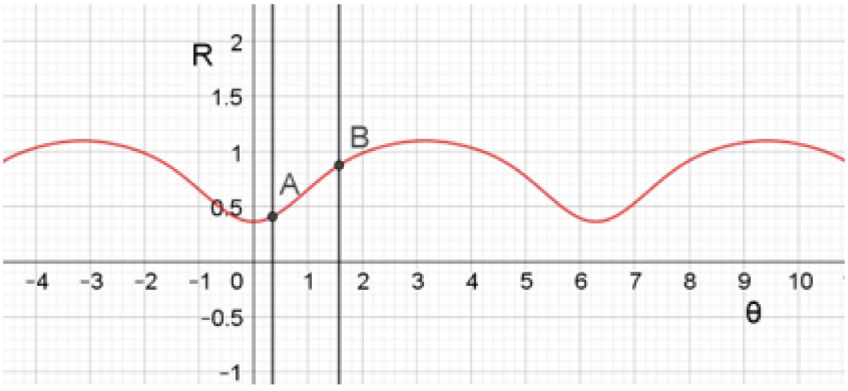


**Fig. 12.** Length of the phasor $R$ as a function of $\theta$.

(2) For clipping height over 20%, the error becomes significant, especially when using 3 phase steps, but also 4 phase steps should be avoided.
(3) For $N \geq 5$, the method is rather immune against a high degree of clipping.

Moreover; by using phasor diagrams, the phase difference between the clipped and the unclipped fringe function is found, and how it is related to the degree of clipping. Since the equation describing this phase difference is anharmonic, we cannot use the standard formula for harmonic functions to calculate the RMS values.

As a final remark, one may infer that the problem of saturation of the camera is easily solved by reducing the camera lens aperture. But then the contrast of the fringes will be reduced which results in a reduction of the signal-to-noise ratio.

## Declaration of competing interest

The authors declare that they have no known competing financial interests or personal relationships that could have appeared to influence the work reported in this paper.

## Acknowledgments

This work was supported by University of Agder, Faculty of Engineering and Science.

## References

[1] K.J. Gåsvik, Optical Metrology, third ed., John Wiley & Sons Chichester, 2002.
[2] S.S. Gorthi, P. Rastogi, Fringe projection techniques: Whither we are? Opt. Lasers Eng. 48 (2010) 133–140.
[3] K. Liu, et al., Gamma model and its analysis for phase measuring profilometry, Meas. Sci. Technol. 26 (2015) 035201.
[4] S. Zhang, S.-T. Yau, Generic nonsinusoidal phase error correction for three-dimensional shape measurement using a digital video projector, Appl. Opt. 46 (2007) 36–43.
[5] J. Yao, et al., Phase error elimination considering gamma nonlinearity, system vibration, and noise for fringe projection profilometry, Opt. Eng. 53 (9) (2014) 094102-1, 7 pages.
[6] B. Pan, et al., Phase error analysis and compensation for nonsinusoidal waveforms in phase-shifting digital fringe projection profilometry, Opt. Lett. 34 (4) (2009) 416–418.
[7] X.-Y. Su, et al., Automated phase-measuring profilometry using defocused projection of a Ronchi grating, Opt. Commun. 94 (1992) 561–573.
[8] B. Chen, S. Zhang, High-quality 3D shape measurement using saturated fringe patterns, Opt. Lasers Eng. 87 (2016) 83–89.
[9] E. Hu, Y. He, W. Wu, Further study of the phase recovering algorithm for partial intensity saturation in digital projection grating phase-shifting profilometry, Optik 121 (2010) 1290–1294.
[10] P. Zhou, X. Liu, Y. He, T. Zhu, Phase error analysis and compensation considering ambient light for phase measuring profilometry, Opt. Lasers Eng. 55 (2014) 99–104.
[11] Z. Qi, et al., Error of image saturation in the structured-light method, Appl. Opt. 57 (2018) 181–188.
[12] C. Waddington, J. Kofman, Modified sinusoidal fringe-pattern projection for variable illuminance in phase-shifting three-dimensional surface-shape metrology, Opt. Eng. 53 (8) (2014) 084109-1, 9 pages.
[13] C.J. Morgan, Least-squares estimation in phase-measurement interferometry, Opt. Lett. 7 (1982) 368–370.
[14] J.E. Greivenkamp, Generalized data reduction for heterodyne interferometry, Opt. Eng. 4 (1984) 350–352.
[15] G. Lai, T. Yatagai, Generalized phase-shifting interferometry, J. Opt. Soc. Amer. A 8 (1991) 822–827.
[16] Schwider, et al., Digital wave-front measuring interferometry: Some systematic error sources, Appl. Opt. 22 (1983) 3421–3432.
[17] K. Creath, Temporal phase measurement methods, in: D.W. Robinson, G.T. Reid (Eds.), Interferogram Analysis, IoP-Publishing Ltd, Bristol, 1993, pp. 94–140.